Scaling of surface roughness in perfectly plastic disordered media

Pallab Barai, Rahul Sampath, Phani Kumar V. V. Nukala, and Srđan Šimunović
Computer Science and Mathematics Division, Oak Ridge National Laboratory, Oak Ridge, Tennessee 37831-6359, USA
(Received 12 August 2010; published 19 November 2010)

This paper investigates surface roughness characteristics of localized plastic yield surface in a perfectly plastic disordered material. We model the plastic disordered material using perfectly plastic random spring model. Our results indicate that plasticity in a disordered material evolves in a diffusive manner until macroscopic yielding, which is in contrast to the localized failure observed in brittle fracture of disordered materials. On the other hand, the height-height fluctuations of the plastic yield surfaces generated by the spring model exhibit roughness exponents similar to those obtained in the brittle fracture of disordered materials, albeit anomalous scaling of plastic surface roughness is not observed. The local and global roughness exponents (ζ_{loc} and ζ, respectively) are equal to each other, and the two-dimensional crack roughness exponent is estimated to be $\zeta_{loc}=\zeta=0.67\pm0.03$. The probability density distribution $p[\Delta h(\ell)]$ of the height differences $\Delta h(\ell)=[h(x+\ell)-h(x)]$ of the crack profile follows a Gaussian distribution.

DOI: 10.1103/PhysRevE.82.056116 PACS number(s): 62.20.mm, 46.50.+a, 62.25.Mn

I. INTRODUCTION

The effect of statistical heterogeneity on the ductile fracture behavior of materials has been a major field of research in the last two decades [1,2]. Unlike brittle fracture, ductile materials develop plasticity as the loading continues to increase. From a macroscopic point of view, continuum plasticity is modeled as a smooth irreversible deformation process using yield surfaces and flow rules derived from flow potential [3]. On the other hand, at microscopic level, plasticity in crystalline materials is explained by the motion of dislocations under an applied stress. Recent theoretical and experimental investigations suggest that crystal plasticity is characterized by large intrinsic spatiotemporal fluctuations with scale-invariant characteristics [2]. Specifically, deformation proceeds through intermittent temporal bursts with power-law size distributions, while spatial deformation patterns and deformation-induced surface morphology are characterized by long-range correlations and self-affine roughness [2].

Coupling these microscopic spatiotemporal fluctuations with the macroscopic continuum plasticity theories has been a challenge for decades. Application of general continuum-based elastoplastic fracture mechanics theories cannot capture the material heterogeneity driven fluctuations in the strength and fracture surface profiles. Statistical models are necessary for this purpose as these models consider the disorder explicitly. In this sense, these statistical models can be used to model material microstructure explicitly [4,5]. Moreover, these models introduce an explicit microstructural length scale that stabilizes the governing continuum equations, which eliminates the usual mesh dependencies observed in fracture simulations using finite element methods. Finally, statistical models play an important role in characterizing the fracture surface roughness. Consequently, over the years, statistical models have been used at the microscopic level to study material yielding in the presence of disorder and to capture these scale-invariant characteristics such as the avalanche bursts and self-affine fracture morphology [1,6–8].

Traditionally, the localization surface obtained in plastic disordered media in the perfect plastic limit is considered to be analogous to the minimum-energy surface [6,9] in a disordered medium. Based on this analogy, the localization surface in a plastic disordered media is expected be a self-affine object with a roughness scaling exponent of $\zeta=\frac{2}{3}$. Alternatively, a well-established technique to study localization surface roughness is the lattice model where the medium is described by a discrete set of bonds with randomly distributed thresholds [10,11]. The bonds can be chosen to be either elastic or elastoplastic in nature. The random thresholds signify either the failure strength of a particular bond in the case of an elastic brittle bond or the yield strength beyond which the behavior of the bond changes from elastic state to plastic state. Recent studies [1] using perfectly plastic random fuse model (PPRFM) suggest that the localization surface obtained in the perfectly plastic limit may not coincide with the minimum-energy surfaces. Specifically, the authors of Ref. [1] note that the yield surfaces obtained using PPRFM exhibit multiaffine scaling below a cutoff length scale, albeit the roughness scaling exponent above this cutoff length scale is in good agreement with that obtained using minimum-energy surface analogy. In terms of lattice models, PPRFM is the simplest scalar representation of elastoplastic continuum. Although the scaling of fracture surfaces using scalar and vectorial representation models such as random fuse, spring, and beam models [12–14] has been shown to be similar for elastic brittle fracture simulations, it is not *a priori* clear whether the same behavior extends for plasticity. Consequently, in this study, we analyze roughness of localization surfaces using perfectly plastic random spring model (PPRSM), which accounts for vectorial representation of elastoplastic continuum.

In addition to the scaling of localization surfaces, we also study localization features of plasticity evolution. Plasticity accumulation in a plastic disordered media is controlled by two competing aspects: disorder and stress concentration or mitigation effects in the vicinity of a plastic bond. When the disorder is strong, plasticity evolves in an uncorrelated manner in the initial stages and thus resembles percolation. As

 ©2010 The American Physical Society

plasticity accumulates and the yield surface starts to develop, some degree of correlation can be expected due to plasticity localization. A natural question to ask concerns the relevance of these correlations as plasticity develops. If correlations are irrelevant one should observe percolation scaling up to macroscopic yielding of the lattice, as in the case of infinite disorder. The interesting question is whether plasticity accumulation follows percolation scaling up to macroscopic yielding, and if not, when does long-range correlations develop and what is its scaling? An understanding of these plastic damage fluctuations at the microscopic scale is necessary for accurately capturing their relevance at macroscopic scale.

This paper is organized as follows. Section II presents the details of perfectly plastic random spring model, which is a vectorial representation of elastoplastic medium. Section III describes the process of plasticity evolution, and Sec. IV presents the surface roughness properties of the yield surface. Section V concludes this paper with a summary of the work presented here. Finally, we note that a complete plasticity behavior of materials is not considered in this paper. In particular, the model presented in here does not consider repeated loading and unloading cycles and strain hardening behavior. This would involve an extension of the present algorithm and will be considered in subsequent study.

II. PERFECTLY PLASTIC RANDOM SPRING MODEL

We consider a PPRSM to investigate surface roughness characteristics of localized plastic yielding surface in a perfectly plastic disordered material. In the PPRSM, we consider an intact two-dimensional diamond-shaped lattice of size $L \times L$ with 45° inclined bonds. The load-displacement characteristics of each of the bonds is described by a perfectly plastic behavior such that the bond is elastic as long as the force in the bond is less than the yield threshold, and it transitions into the plastic state once the force exceeds the yield threshold. Moreover, we assume that once a bond enters plastic state, it remains in perpetual plastic state; that is, there is no unloading of a plastic bond due to stress redistributions and loading (see Ref. [6]). The main difference between traditionally used random spring model (RSM) for brittle fracture [10,13] and the PPRSM is that once the force threshold in the bond is reached, the force in the PPRSM bond remains constant at its threshold value, while the force in the traditional RSM drops to zero. Further increase in external loading does not increase forces in bonds that are already in "plastic" state. Once a connected yield surface is developed, any further increase in loading causes the lattice to "flow." At this point the lattice is declared to have reached its macroscopic plastic limit and the surface with all yielded bonds is called the yield surface.

In the PPRSM, we start with a fully intact lattice system with bonds having the same conductance until the yield threshold and zero conductance there afterward. Bond yield thresholds t are randomly distributed based on a threshold probability distribution $p(t)$. In this paper, we assume a uniform distribution between [0,1] for bond thresholds; that is, $p(t) \equiv 1$. Periodic boundary conditions are imposed in the horizontal direction, and a constant unit displacement difference is applied between the top and the bottom of lattice system.

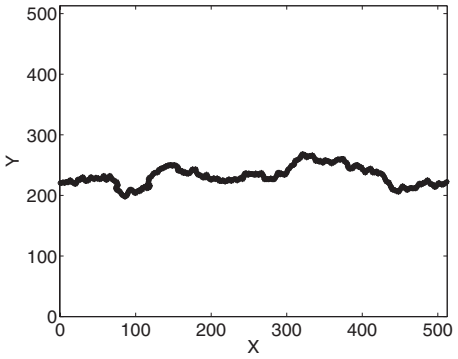

FIG. 1. Yield surface obtained using the RSM for a lattice of size $L=512$.

In the following, we adopt the tangent algorithm proposed in Ref. [6] to simulate plastic yielding in a lattice system. At the beginning of the simulation, we initialize the forces $f_j^{(0)}$ in each of the jth spring to zero. Subsequently, during each of the $(n+1)$th load step (where $n=0,1,2,\ldots$), a unit displacement $\Delta=1$ is applied at the top of the lattice system and the equilibrium equations are solved to determine the force in each of the springs. For each bond j, the ratio between the force f_j obtained during the $(n+1)$th step and the remaining breaking threshold $(t_j-f_j^{(n)})$ is evaluated, and the state of the bond j_c having the largest value, $\lambda=\max_j[f_j/(t_j-f_j^{(n)})]$, is changed from elastic to plastic. Subsequently, forces in each of the elastic springs are updated as $f_j^{(n+1)}=f_j^{(n)}+(f_j/\lambda)$. For the next step, the bond j_c that became plastic is removed from lattice system irreversibly since we assume that once a bond enters plastic state, it remains in that state forever, and consequently cannot sustain any further increase in its member force. This step is equivalent to removing the j_c bond contribution from the global stiffness matrix. This process of yielding one bond at a time is continued until a connected plastic surface forms such that the entire lattice starts to flow even under infinitesimal external force. That is, the lattice stiffness becomes zero at this point.

Figure 1 shows a typical yield surface obtained using the PPRSM for a lattice system of size $L=512$. At each load step, we solve the equilibrium equations using the multiple-rank sparse Cholesky factorization updating algorithm presented in Ref. [15]. In comparison with the Fourier accelerated iterative schemes used for modeling lattice breakdown [16], this algorithm significantly reduced the computational time required for solving large lattice systems. In this paper, we consider lattice system sizes up to $L=256$ for studying the surface roughness scaling laws in plastic disordered media. For all the lattice system sizes, the number of sample configurations, N_{config}, used is excessively large ($N_{config}=10\,000$) to reduce the statistical error in the numerical results.

III. PLASTICITY EVOLUTION

In the following, we investigate plasticity evolution and its localization by analyzing plasticity profiles at different

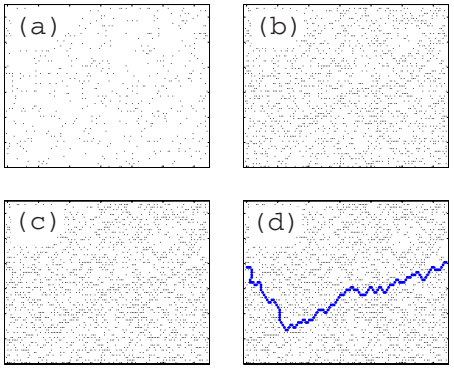

FIG. 2. (Color online) Snapshots of plasticity evolution and the yield surface in a typical simulation of size $L=64$. A total of 2260 bonds have entered perfectly plastic state before macroscopic yielding. Boxes (a)–(d) represent the snapshots of plasticity in the lattice after n_b bonds have become perfectly plastic. (a) $n_b=500$, (b) $n_b=1600$, (c) $n_b=2000$, and (d) $n_b=2260$ (macroscopic yield line appears). The solid line in box (d) signifies the macroscopic yield line.

stages of simulation. For the uniform disorder case, our PPRSM simulations show a substantial amount of plasticity accumulation prior to macroscopic yielding of lattice. Figure 2 presents snapshots of plasticity evolution and the yield surface formation in a typical diamond lattice system of size $L=64$. A total of 2260 bonds have become perfectly plastic before macroscopic yielding of the lattice occurs. The solid line in the last snapshot in Fig. 2 represents the macroscopic yield surface.

Figure 3 displays the damage profile $p(y)$ at failure in a typical simulation. Based on the data from a single sample, it is difficult to assess from these curves the extent of localization. It is clear that plasticity evolves in a diffusive manner in the initial stages of loading as plasticity evolution at this stage is dominated by material disorder. If the effects of

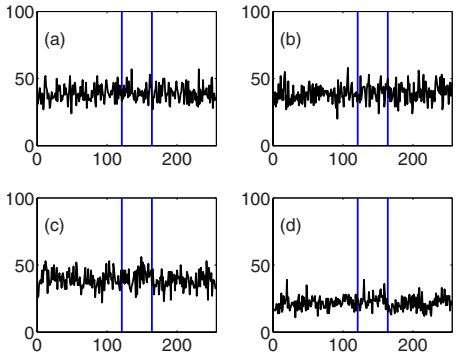

FIG. 3. (Color online) Evolution of plasticity in a lattice of size $L=256$. In each of the subplots, the abscissa refers to the y coordinate of the lattice section and the ordinate is the number of plastic springs in that section. In this simulation a total of 35 593 springs became plastic before the lattice yielded. Plot (a) refers to damage profile after the first 10 000 springs yielded. (b) Between 10 000 and 20 000 springs yielded. (c) Between 20 000 and 30 000 springs became plastic. (d) Between 30 000 and the macroscopic yield of the lattice (35 593 springs are plastic). The two vertical lines show the range in which the final yield surface developed. No localization of plasticity is observed in these figures.

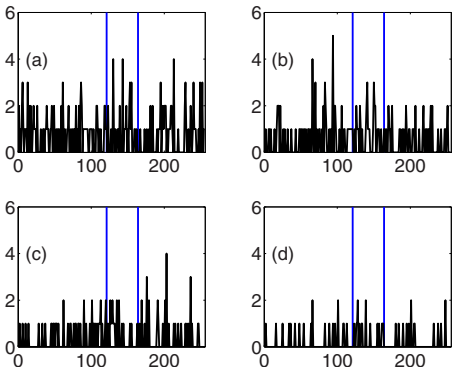

FIG. 4. (Color online) Evolution of plasticity in the late stages of simulation in a lattice of size $L=256$. In each of the subplots, the abscissa refers to the y coordinate of the lattice section and the ordinate is the number of plastic springs in that section. (a) Between the last 500 and last 300 springs that yielded. (b) Between the last 300 and last 150 springs that entered plastic state. (c) Between last 150 and last 50 springs that entered plastic state. (d) Last 50 springs before final yield of the lattice. Once again, the two vertical lines show the range in which the final yield surface developed. No effect of stress concentration is observed even during these late stages of yielding.

stress modification around the plastic tips were to be significant, it is conceivable that we observe localization during later stages of loading. Consequently, we have plotted the plastic damage profiles during the late stages of loading. Figure 4 presents the evolution of plasticity during the later stages of loading in a typical sample. Even at this stage, localization is not apparent to the naked eye.

To investigate this further, in the following, we present a quantitative description of the localization process by averaging different realizations over many samples. Averaging the profiles is a delicate task since localization, even if it occurs, does not necessarily take place in the center, but can in principle occur anywhere along the length of the lattice. Thus, one cannot perform a simple average because this would yield a flat average profile irrespective of the individual profile shapes in a single realization. In Ref. [17], the authors proposed to first shift the profiles, so that they are centered at the maximum and then average. This method emphasizes the noise too much, yielding a spurious cusp in the center. Another possibility is to shift instead by the center of mass of the plasticity damage or, to avoid any effects due to shifting, one can use the Fourier method [18].

We first consider the plasticity accumulated up to macroscopic yielding by shifting the data by the center-of-mass method. The result displayed in Fig. 5 for the uniform disorder distribution clearly shows that there is no localization at macroscopic yielding. Although the profile is not completely flat for small scales, it flattens more and more as the lattice size is increased. We tend thus to attribute the apparent profile for small systems to system size effects.

To obtain additional confirmation of these results, we perform a Fourier analysis of the $p(y)$ profiles, thus avoiding any possible bias due to center-of-mass shifting. We first compute the magnitude of the Fourier transform for each realization and then average over disorder. If the plastic dam-

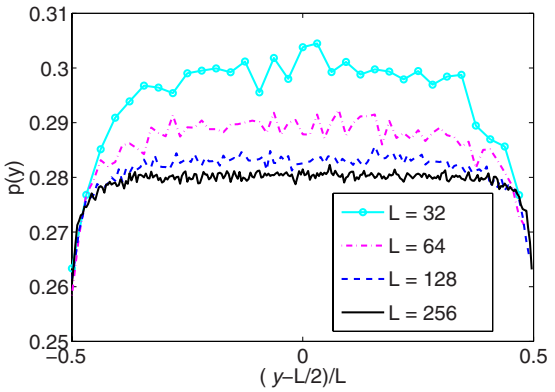

FIG. 5. (Color online) Average plastic damage profiles at macroscopic yielding obtained by first centering the data around the center of mass of the plastic damage and then averaging over different samples. The data correspond to uniformly distributed disorder.

age profiles were to be really uniform, we expect to see a delta distribution in the Fourier space. This result applies to infinite system and finite-size deviations, and other problems of the discrete Fourier transform are expected to affect the data. Nonetheless, as shown in Fig. 6, we note that all the curves follow a delta distribution reasonably well, while the tails represent the boundary effects due to nonperiodicity of plastic damage profiles in the y direction.

In addition to the above analysis of plastic damage profiles, at the end of simulation, we have also analyzed the plastic damage profiles at regular intervals. Specifically, we have divided the simulation into six equal segments and averaged the corresponding plastic damage profiles over different samples. As before, averaging is done by shifting the plastic damage profiles by the center of mass. Figure 7 presents the averaged plastic damage profiles at regular intervals of PPRSM simulation. The data in Fig. 7 show that there is no localization even in the late stages of simulation. The plastic damage profiles flatten out as the lattice system size is increased, and the apparent profile for small systems is due to system size effects.

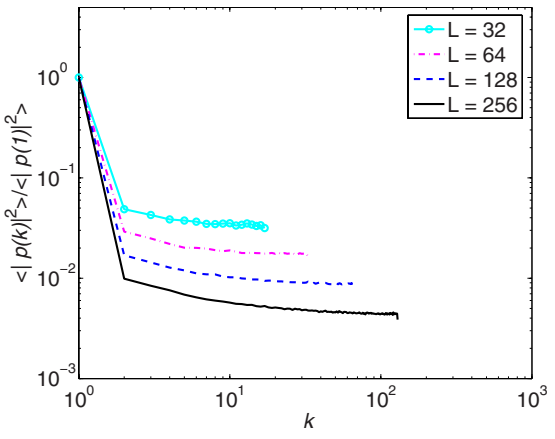

FIG. 6. (Color online) Average power spectra of plastic damage profiles at macroscopic yielding. Fourier transform of each of the plastic damage profiles is averaged over different samples.

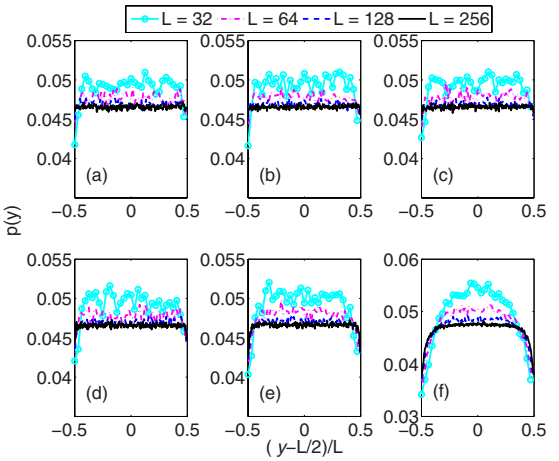

FIG. 7. (Color online) Average plastic damage profiles at six regular intervals of simulation. Averaging of the profiles is done by first centering the data around the center of mass of the plastic damage and then averaging over different samples. The data show that localization of plastic damage does not occur even in the late stages of simulation.

IV. YIELD SURFACE ROUGHNESS

In this section, we investigate the roughness of the yield surface obtained from PPRSM simulations. Once the sample has failed, we identify the final crack, which typically displays dangling ends and jumps in the profile (see Fig. 8). We remove them and obtain a single valued crack line $h(x)$ as shown in Fig. 1, where $x \in [0,L]$, and $h(x)$ represents the local transverse position of the crack line at each x. For self-affine cracks, the local width $w(\ell) \equiv \langle \Sigma_x [h(x) - (1/\ell)\Sigma_X h(X)]^2 \rangle^{1/2}$, where the sums are restricted to regions of length ℓ and the average is over different realizations, scales as $w(\ell) \sim \ell^{\zeta}$ for $\ell \ll L$ and saturates to a value $W = w(L) \sim L^{\zeta}$ corresponding to the global width. The power spectrum $S(k) \equiv \langle \hat{h}_k \hat{h}_{-k} \rangle / L$, where $\hat{h}_k \equiv \Sigma_x h(x) \exp i(2\pi x k/L)$, decays as $S(k) \sim k^{-(2\zeta+1)}$. When anomalous scaling is present [19–21], the exponent describing the system size dependence of the surface *differs* from the local exponent measured for a fixed system size L. In particular, the local width scales as

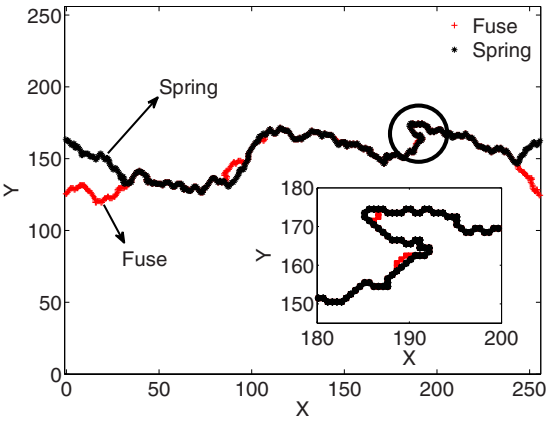

FIG. 8. (Color online) Jumps in crack profile that arise due to solid-on-solid projection of yield surface.

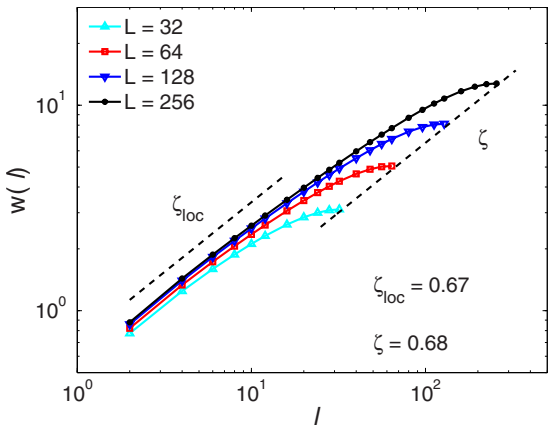

FIG. 9. (Color online) Scaling of yield surface width $w(\ell)$ with window size ℓ for system sizes $L=32,64,128,256$. The analysis are conducted on the original yield surface profiles with jumps. The local and global roughness exponents are obtained as $\zeta_{loc}=0.67$ and $\zeta=0.68$, respectively. The very close resemblance between the values of local and global roughness exponents proves that there is very little anomalous scaling present in the yield surface profile obtained using PPRSM.

$w(\ell) \sim \ell^{\zeta_{loc}} L^{\zeta-\zeta_{loc}}$, so that the global roughness W scales as L^{ζ} with $\zeta > \zeta_{loc}$. Consequently, the power spectrum scales as $S(k) \sim k^{-(2\zeta_{loc}+1)} L^{2(\zeta-\zeta_{loc})}$.

Figure 9 presents the scaling of yield surface width $w(\ell)$ with window size ℓ. The data presented in Fig. 9 indicate that the local roughness exponent is $\zeta_{loc}=0.67$, while the global roughness exponent has a value of $\zeta=0.68$. We have also investigated the power spectra $S(k)$ of the crack profiles (see Fig. 10). Collapse of the power spectra for different system sizes can be observed. The slope of the plots in Fig. 10 is obtained as $-(2\zeta_{loc}+1)=-2.29$, which implies that the local roughness exponent from the power spectrum analysis has a value of $\zeta_{loc}=0.65$ and is consistent with the roughness exponent estimation based on yield surface width data shown in Fig. 9.

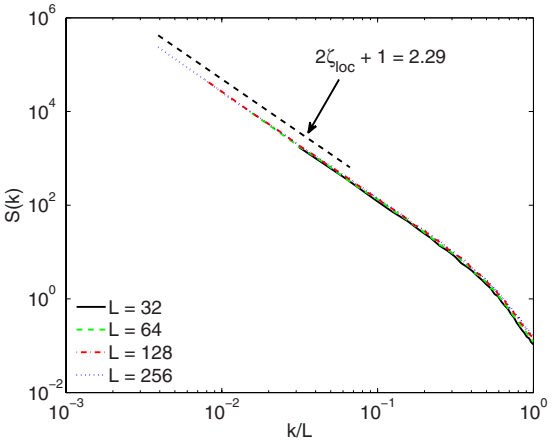

FIG. 10. (Color online) Scaling of power spectrum $S(k)$ of the yield surface profile for system sizes $L=32,64,128,256$. The jumps within the profile are not removed explicitly. The data collapse very well for different system sizes. The local roughness exponent is obtained as $\zeta_{loc}=0.65$, which is very close to that observed using yield surface width analysis as shown in Fig. 9.

The self-affine property of the yield surface profile also implies that the probability density distribution $p[\Delta h(\ell)]$ of the height differences $\Delta h(\ell)=[h(x+\ell)-h(x)]$ of the yield surface profile follows the relation

$$p[\Delta h(\ell)] \sim \langle \Delta h^2(\ell) \rangle^{-1/2} f\left(\frac{\Delta h(\ell)}{\langle \Delta h^2(\ell) \rangle^{1/2}} \right). \tag{1}$$

Noting that periodicity in yield surface profiles is analogous to return-to-origin excursions arising in stochastic processes, we propose the following ansatz for the local width $\langle \Delta h^2(\ell) \rangle^{1/2}$ in height differences $\Delta h(\ell)$:

$$\langle \Delta h^2(\ell) \rangle^{1/2} = \langle \Delta h^2(L/2) \rangle^{1/2} \phi\left(\frac{\ell}{L/2} \right), \tag{2}$$

with $\langle \Delta h^2(L/2) \rangle^{1/2} = L^{\zeta}$. For periodic profiles, the function $\phi(\frac{\ell}{L/2})$ is symmetric about $\ell=L/2$ and is constrained such that $\phi(\frac{\ell}{L/2})=0$ at $\ell=0$ and $\ell=L$, and $\phi(\frac{\ell}{L/2})=1$ at $\ell=L/2$. Based on these conditions, a scaling ansatz of the form

$$\left[\frac{\langle \Delta h^2(\ell) \rangle^{1/2}}{\langle \Delta h^2(L/2) \rangle^{1/2}} \right]^{1/\zeta_{loc}} + \frac{(\ell - L/2)^2}{(L/2)^2} = 1, \tag{3}$$

similar to stochastic excursions or bridges, can be proposed for $\langle \Delta h^2(\ell) \rangle^{1/2}$, which implies a functional form

$$\phi\left(\frac{\ell}{L/2} \right) = \left[1 - \left(\frac{(\ell - L/2)}{L/2} \right)^2 \right]^{\zeta_{loc}}, \tag{4}$$

for $\phi(\frac{\ell}{L/2})$ that is satisfied to a good approximation by our numerical results. This scaling ansatz results in anomalous scaling when $\zeta_{loc} \neq \zeta$. Upon further simplification, Eq. (4) results in

$$\phi\left(\frac{\ell}{L/2} \right) = 4^{\zeta_{loc}} \left(\frac{\ell}{L} \right)^{\zeta_{loc}} \left(1 - \frac{\ell}{L} \right)^{\zeta_{loc}}, \tag{5}$$

which along with $\langle \Delta h^2(L/2) \rangle^{1/2} = L^{\zeta}$ and Eq. (2) shows how anomalous scaling arises and how local and global roughness exponents ζ_{loc} and ζ can be computed based on numerical results.

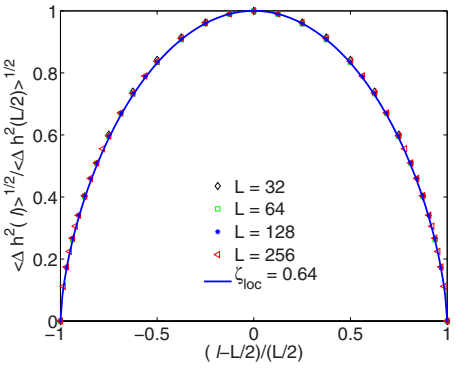

FIG. 11. (Color online) Scaling of $\langle \Delta h^2(\ell) \rangle^{1/2}$ with window size ℓ shows collapse of data onto Eq. (4) with $\zeta_{loc}=0.64$. The data presented are for system sizes $L=32,64,128,256$. The local roughness exponent ($\zeta_{loc}=0.64$) is consistent with the estimated roughness exponents using the crack width (Fig. 9) and power spectrum (Fig. 10) analyses.

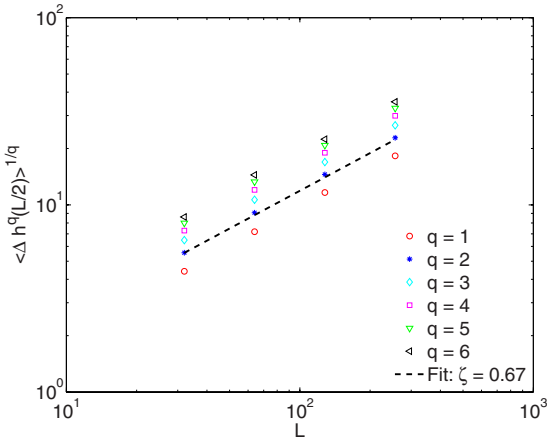

FIG. 12. (Color online) Scaling of $\langle \Delta h^q(L/2) \rangle^{1/q}$ with system size L with a scaling exponent of $\zeta=0.67$. The global roughness exponent is consistent with the roughness exponent ($\zeta=0.68$) obtained in Fig. 9.

Figure 11 presents the scaling of $\langle \Delta h^2(\ell) \rangle^{1/2}$ based on the above ansatz [Eqs. (2) and (4)]. Collapse of the $\langle \Delta h^2(\ell) \rangle^{1/2} / \langle \Delta h^2(L/2) \rangle^{1/2}$ data for different system sizes $L=[32,64,128,256]$ and window sizes $\ell \leq L$ onto a scaling form given by Eq. (4) with $\zeta_{loc}=0.64$ can be clearly seen in Fig. 11.

The global roughness exponent of the yield surface profiles can be estimated by analyzing $\langle \Delta h^q(L/2) \rangle^{1/q}$ scaling. Figure 12 presents the scaling of $\langle \Delta h^q(L/2) \rangle^{1/q}$ for $q=1$ to $q=6$. The data presented in this figure indicate that the slopes of the data for moments $q=1-6$ of $\Delta h(L/2)$ are identical. It should also be noted that $\langle \Delta h^q(L/2) \rangle^{1/q} \sim L^{\zeta}$, with $\zeta=0.67$. Considering the margin of error in the calculations, the methods of estimation, and the approximately similar values for local and global roughness exponents, we conclude that yield surface profiles do not exhibit anomalous scaling. This is in contrast with traditional two-dimensional fracture simulations [12], where anomalous scaling of two-dimensional fracture profiles has been observed.

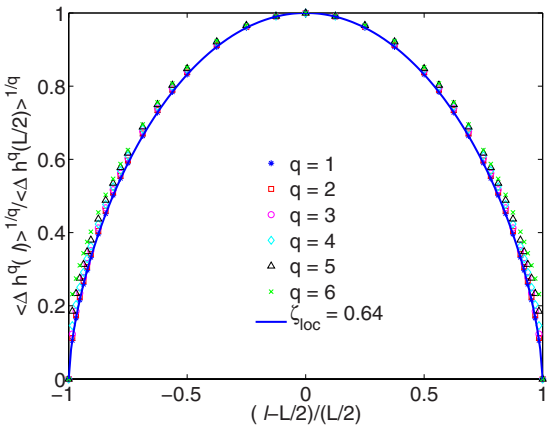

FIG. 13. (Color online) Scaling of $\langle \Delta h^q(\ell) \rangle^{1/q}$ with window size ℓ for a system of size $L=256$. The local roughness exponent is estimated to be $\zeta_{loc}=0.64$. The data for different values of q do not collapse onto each other especially at smaller length scales, which suggests the presence of multiscaling of yield surface profile possibly due to the presence of jumps in the profile.

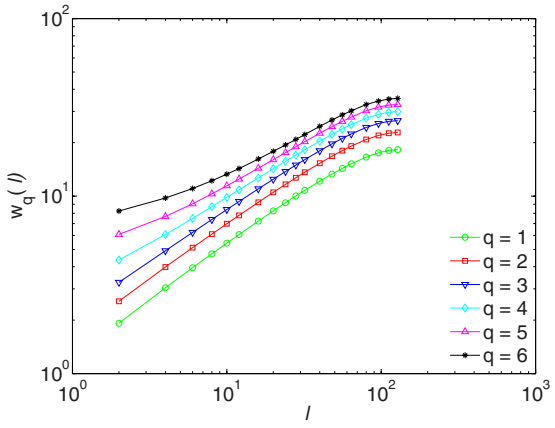

FIG. 14. (Color online) Scaling of qth-order correlation function $C_q(\ell)$ for a system of size $L=256$ under periodic boundary conditions. Because of periodicity, the data for window sizes $\ell > L/2$ are symmetric about $\ell=L/2$. Hence, window sizes of only up to $\ell=L/2$ have been shown in the figure. Fanning out of the data below a cutoff length scale suggests multiscaling, albeit the reason behind this effect may be the jumps in the profile (see Ref. [14]).

In addition to the above anomalous scaling analysis, in the following, we investigate multiaffine scaling of yield surface profiles. Figure 13 presents the $\langle \Delta h^q(\ell) \rangle^{1/q} / \langle \Delta h^q(L/2) \rangle^{1/q}$ data for $q=1$ to $q=6$. The data collapse is not perfect especially for small window sizes $\ell \ll L/2$, albeit a reasonable collapse of the data is observed at length scales above a cutoff length. Scaling of the data at these intermediate length scales suggests that a local roughness exponent of $\zeta_{loc}=0.64$, same as that obtained from Fig. 11, represents an adequate fit for the data. As pointed out in Ref. [12], noncollapse of the data at smaller length scales $\ell \ll L/2$ might arise due to jumps in the yield surface profile. The removal of

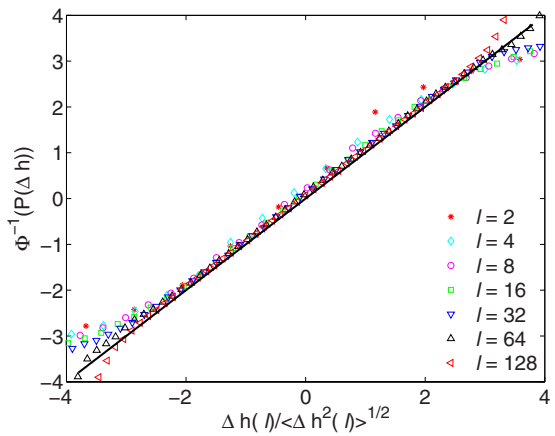

FIG. 15. (Color online) Plots of cumulative probability distributions $P[\Delta h(\ell)]$ of the height differences $\Delta h(\ell)=[h(x+\ell)-h(x)]$ of the yield surface profile $h(x)$ for various bin sizes ℓ on a normal paper. Φ^{-1} denotes inverse Gaussian. This $P[\Delta h(\ell)]$ distribution is obtained for a system of size $L=256$ with window lengths $\ell=[2,4,8,16,32,64,128]$. The collapse of the profiles onto a straight line with unit slope indicates that a Gaussian distribution is adequate to represent $P[\Delta h(\ell)]$. The deviation of some data points from the straight line with unit slope can be attributed to the presence of the small jumps within the yield surface profiles.

these jumps from the yield surface profiles often eliminates this artifact of multiaffine scaling.

To further investigate multiscaling behavior of surface roughness, we study the scaling of the qth-order correlation function $C_q(\ell)=\langle|h(x+\ell)-h(x)|^q\rangle^{1/q}$. Figure 14 shows the scaling of data for $q=1$ to $q=6$. The window length ℓ ranges from $\ell=2$ to $\ell=L/2$. Because of periodicity the data for $\ell > L/2$ are symmetric about $\ell=L/2$. Figure 14 shows that the data fan out at smaller length scales below a cutoff length scale. This feature is a characteristic signature of multiaffine scaling and is in agreement with the data shown in Fig. 13. Multiscaling at small scales was also observed in the perfectly plastic random fuse model simulations [1]. However, as in traditional fracture simulations, we believe that multiscaling vanishes once the jumps in the profile are removed.

In the following, we investigate the probability density $p[\Delta h(\ell)]$ of height differences $\Delta h(\ell)$. In Refs. [22–24], the $p[\Delta h(\ell)]$ distribution is shown to follow a Gaussian distribution above a cutoff length scale, and the deviations away from Gaussian distribution in the tails of the distribution have been attributed to finite jumps in the crack profiles. A similar behavior from the yield surface profiles obtained using the PPRSM can be expected. Self-affine scaling of $p[\Delta h(\ell)]$ as given by Eq. (1) implies that the cumulative distribution $P[\Delta h(\ell)]$ scales as $P[\Delta h(\ell)] \sim P[\Delta h(\ell)/\langle\Delta h^2(\ell)\rangle^{1/2}]$. Figure 15 presents the raw data of cumulative probability distributions $P[\Delta h(\ell)]$ of the height differences $\Delta h(\ell)$ on a normal or Gaussian paper for bin sizes $\ell < L$. The data are for a system size of $L=256$ with window lengths $\ell=[2,4,6,8,16,32,64,128]$. The collapse of the data onto a straight line with unit slope indicates the adequacy of Gaussian distribution for $P[\Delta h(\ell)]$. Deviations from the Gaussian pattern are observed at the tails of the distribution, which is once again due to the presence of jumps within the yield surface profiles.

V. DISCUSSION

In summary, the analysis and results presented in this paper indicate that surface roughness characteristics of localized plastic yield surface in perfectly plastic disordered material exhibit roughness exponents similar to those obtained in the brittle fracture of disordered materials, albeit anomalous scaling of plastic surface roughness is not observed. The local and global roughness exponents (ζ_{loc} and ζ, respectively) are equal to each other, and the two-dimensional crack roughness exponent is estimated to be $\zeta_{loc}=\zeta=0.67\pm0.03$. This result is in agreement with the roughness estimates obtained using the perfectly plastic random fuse model [1]. Multiaffine scaling of yield surface lines is observed below a cutoff length scale as shown in Fig. 8. However, as with brittle random fuse and beam models we have studied earlier [14], multiscaling at small scales appears to be an artifact of jumps in the crack profiles. In Ref. [14], we have analyzed the scaling of crack profiles after eliminating the jumps in the crack profiles. Our observation was that once we removed the jumps in the profiles, multiscaling vanished. In this sense, we conclude that there are no real physical arguments (physical processes) for the existence of multiscaling at small scales. The probability density distribution $p[\Delta h(\ell)]$ of the height differences $\Delta h(\ell)=[h(x+\ell)-h(x)]$ of the crack profile follows a Gaussian distribution.

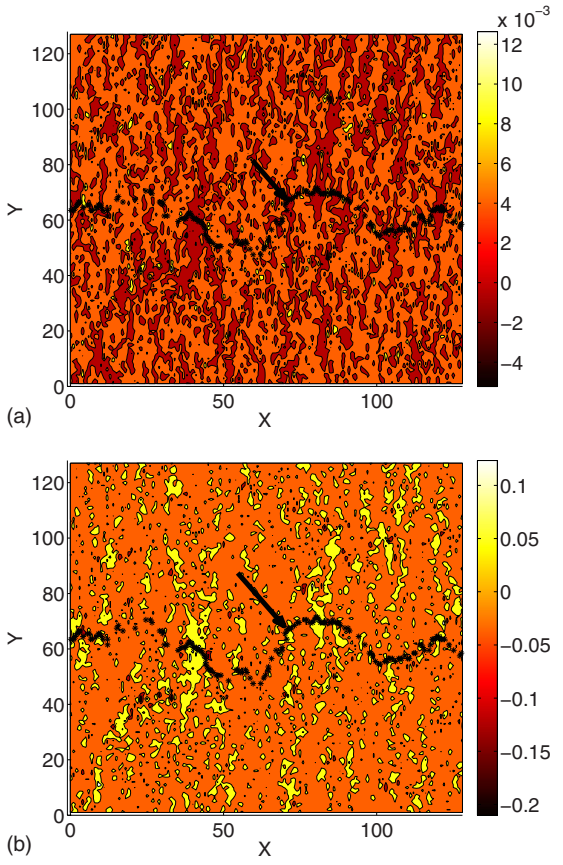

FIG. 16. (Color online) A typical force distribution within a $L\times L$ spring lattice system of size $L=128$ under (a) elastic and (b) plastic loading conditions. In this simulation, a total of 9460 springs became perfectly plastic when the macroscopic yielding of the lattice occurred. The snapshot of force distribution corresponds to a scenario when 5000 bonds entered plastic state. The arrow in the figure identifies the partially formed yield surface segment that is part of the final yield surface.

In Sec. III, we presented plasticity evolution in a disordered material and noted that accumulation of plasticity is dominated by disorder. Specifically, we noted that long-range correlations of plasticity accumulation are absent in these simulations, i.e., localization of plasticity damage was not observed even at late stages of simulation. It is in this sense that plasticity accumulation is akin to percolation with infinite disorder. This is in contrast with fracture and damage accumulation in elastic disordered media, where damage accumulation is dominated by disorder up to the peak load of stress-strain curve and localization of damage dominated by stress concentration is seen in the postpeak regime [18].

To further investigate this difference in behavior, we first decompose the problem into "elastic" and plastic loading cases and analyze the force distribution in the lattice under each of these loading scenarios. Whenever a bond enters a plastic state, it carries current equal to its yield threshold value, and its "tangent" conductance in the plastic state is zero. In this state, the problem is identical to replacing the

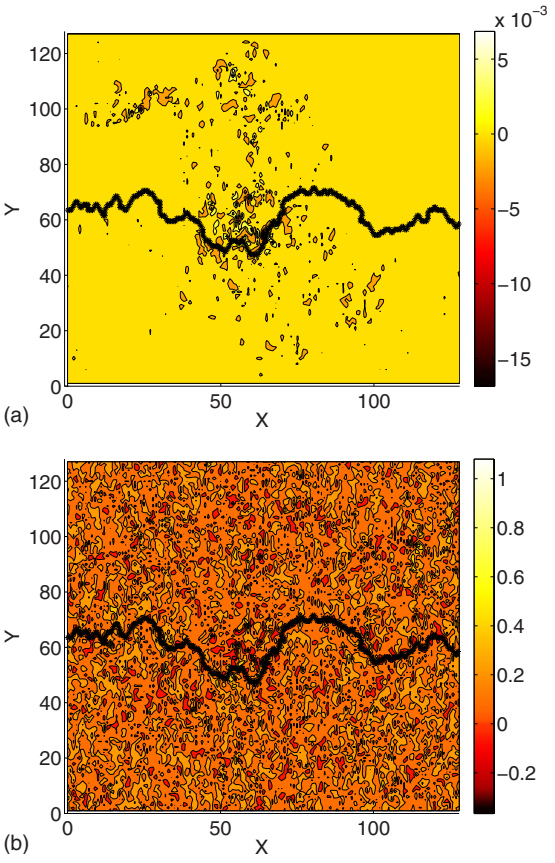

FIG. 17. (Color online) A typical force distribution within a $L \times L$ spring lattice system of size $L=128$ under (a) elastic and (b) plastic loading conditions. In this simulation, a total of 9460 springs became perfectly plastic when the macroscopic yielding of the lattice occurred. The snapshot of force distribution corresponds to a scenario when 9450 bonds entered plastic state. The solid line in the middle denotes the final yield surface.

plastic bond with two nodal forces at the corresponding nodes of the bond. In this sense, the problem is decomposed into an elastic fracture problem, wherein the plastic bond is removed, and a plastic problem with only applied forces at the nodes of the plastic bond. The total force in each of the bonds is obtained by the superposition of forces in the elastic fracture problem and the forces from the plastic problem with nodal loads [25].

Figures 16 and 17 present typical force distribution under elastic and plastic loading conditions at intermediate and final macroscopic yielding stages of simulation. The force distributions in Figs. 16(a) and 17(a) indicate that most of the springs in the lattice show very small force under elastic loading, although high concentration of forces is observed around the crack consistent with fracture propagation in elastic disordered material. On the other hand, the plastic force distribution in Figs. 16(b) and 17(b) is more or less uniform throughout the lattice, and there is no apparent stress concentration around the final yield surface under plastic loading conditions. Moreover, the magnitude of forces in Fig. 17(b) is much higher than that in Fig. 17(a). Consequently, the stress concentration around the cracks in Fig. 17(a) is smeared by the uniform force distribution in Fig. 17(b). This explains why there is no localization of plastic damage even during late stages of simulation. Moreover, localization of plasticity in continuum materials is observed when the governing equations of material lose their ellipticity condition. This is typically the case when the material undergoes large deformations (such as in sheet rolling), is under high strain rate loading, is in the presence of some sort of material softening (such as phase transitions, microstructural damage due to nucleation and growth of voids, large irradiated swelling, etc.), or when the plastic yield surface exhibits corners. Since the simulations considered in the present study do not incorporate any of the above-mentioned phenomena, localization of plasticity is not observed in our simulations. On the other hand, it would be interesting to study whether localization is observed in disordered materials with brittle damage and perfect plasticity.

ACKNOWLEDGMENTS

This research was sponsored by the Mathematical, Information and Computational Sciences Division, Office of Advanced Scientific Computing Research, U.S. Department of Energy under Contract No. DE-AC05-00OR22725 with UT-Battelle, LLC.

[1] C. B. Picallo, J. M. Lopez, S. Zapperi, and M. J. Alava, Phys. Rev. Lett. **103**, 225502 (2009).
[2] M. Zaiser, Adv. Phys. **55**, 185 (2006).
[3] *Mechanics of Solid Materials*, edited by J. Lemaitre and J. L. Chaboche (Cambridge University Press, Cambridge, England, 1990).
[4] J. G. M. Van Mier and M. R. A. Van Vliet, Eng. Fract. Mech. **70**, 2281 (2003).
[5] J. E. Bolander and N. Sukumar, Phys. Rev. B **71**, 094106 (2005).
[6] S. Roux and A. Hansen, J. Phys. II **2**, 1007 (1992).
[7] E. T. Seppälä, V. I. Räisänen, and M. J. Alava, Phys. Rev. E **61**, 6312 (2000).
[8] V. I. Räisänen, M. J. Alava, and R. M. Nieminen, Phys. Rev. B **58**, 14288 (1998).
[9] A. Hansen, E. L. Hinrichsen, and S. Roux, Phys. Rev. Lett. **66**, 2476 (1991).
[10] M. J. Alava, P. K. V. V. Nukala, and S. Zapperi, Adv. Phys. **55**, 349 (2006).
[11] *Statistical Models for the Fracture of Disordered Media*, edited by H. J. Herrmann and S. Roux (North-Holland, Amsterdam, 1990).
[12] P. K. V. V. Nukala, S. Zapperi, M. J. Alava, and S. Šimunović, Int. J. Fract. **154**, 119 (2008).
[13] Phani Kumar V. V. Nukala, S. Zapperi, and S. Šimunović, Phys. Rev. E **71**, 066106 (2005).

[14] P. K. V. V. Nukala, S. Zapperi, M. J. Alava, and S. Šimunović, Phys. Rev. E **78**, 046105 (2008).
[15] P. K. V. V. Nukala and S. Simunovic, J. Phys. A **36**, 11403 (2003).
[16] G. G. Batrouni and A. Hansen, Phys. Rev. Lett. **80**, 325 (1998).
[17] F. Reurings and M. J. Alava, Eur. Phys. J. B **47**, 85 (2005).
[18] P. K. V. V. Nukala, S. Simunovic, and S. Zapperi, J. Stat. Mech.: Theory Exp. (2004), P08001.
[19] J. M. López, M. A. Rodríguez, and R. Cuerno, Phys. Rev. E **56**, 3993 (1997).
[20] J. M. López and J. Schmittbuhl, Phys. Rev. E **57**, 6405 (1998).
[21] S. Morel, J. Schmittbuhl, J. M. López, and G. Valentin, Phys. Rev. E **58**, 6999 (1998).
[22] L. I. Salminen, M. J. Alava, and K. J. Niskanen, Eur. Phys. J. B **32**, 369 (2003).
[23] M. J. Alava, P. K. V. V. Nukala, and S. Zapperi, J. Stat. Mech.: Theory Exp. (2006), L10002.
[24] S. Santucci, K. J. Maloy, A. Delaplace, J. Mathiesen, A. Hansen, Jan Oistein Haavig Bakke, J. Schmittbuhl, L. Vanel, and P. Ray, Phys. Rev. E **75**, 016104 (2007).
[25] P. K. V. V. Nukala, P. Barai, and R. S. Sampath, J. Stat. Mech.: Theory Exp. (2010), P11004.